

INtra-procedural ultraSound Imaging for DEtermination of atrial wall thickness and acute tissue changes after isolation of the Pulmonary Veins with radiofrequency, cryoballoon or laser balloon energy: the INSIDE PVs Study

Short title: INSIDE PVs study

Authors: Milena Leo^a, MD, Giovanni Luigi De Maria^a, MD, PhD, Andre Briosas e Gala^a, MD, Michael Pope^a, MD, Abhirup Banerjee^b, PhD, Andrew Kelion^a, MD, Michala Pedersen^a, MD, PhD, Kim Rajappan^a, MD, Matthew Ginks^a, MD, Yaver Bashir^a MD, Ross J Hunter^c, MD, PhD, Tim Betts^d, MD.

a: Oxford University Hospitals NHS Foundation Trust, Oxford, UK

b: Division of Cardiovascular Medicine, Radcliffe Department of Medicine, University of Oxford, Oxford, UK

c: Barts Health Centre, London, UK

d: Oxford NIHR Biomedical Research Centre

Word count: 4974

Corresponding author:

Prof Tim R Betts

Consultant Cardiologist and Electrophysiologist

Oxford University Hospitals NHS Foundation Trust, Headley Way, Oxford (UK) OX3 7BA

email address: epdoctors@ouh.nhs.uk

Conflict of interests statements:

ABSTRACT

Introduction. Preliminary data in human suggest that both Intracardiac echocardiography (ICE) and Intravascular ultrasound (IVUS) can be used for real-time information on the left atrial (LA) wall thickness and on the acute tissue changes produced by energy delivery.

Objective. This pilot study was conducted to compare ICE and IVUS for real-time LA wall imaging and assessment of acute tissue changes produced by radiofrequency (RF), cryo and laser catheter ablation.

Methods Patients scheduled for RF, cryoballoon or laser balloon Pulmonary Vein Isolation (PVI) catheter ablation were enrolled. Each pulmonary vein (PV) was imaged immediately before and after ablation with either ICE or IVUS. The performance of ICE and IVUS for imaging were compared. Pre- and post-ablation measurements (lumen and vessel diameters, areas and sphericity indexes, wall thickness and muscular sleeve thickness) were taken at the level of each PV ostium.

Results A total of 48 PVs in 12 patients were imaged before and after ablation. Compared to IVUS, ICE showed higher imaging quality and inter-observer reproducibility of the PV measurements obtained. Acute wall thickening suggestive of oedema was observed after RF treatment ($p = 0.003$) and laser treatment ($p = 0.003$) but not after cryoablation ($p = 0.69$).

Conclusions Our pilot study suggests that ICE is preferable to IVUS for LA wall thickness imaging at the LA-PV junctions during ablation. Ablation translates in acute wall thickening when using RF or laser energy, but not after cryoenergy delivery. Larger studies are required to confirm these preliminary findings.

Keywords: intracardiac echocardiography, intravascular ultrasound, left atrial wall thickness; acute wall changes after ablation, radiofrequency energy, cryo energy, laser energy.

Abbreviations: AF = atrial fibrillation; ICE = Intracardiac echocardiography; IQR = Interquartile range; IVUS= Intravascular ultrasound; LA = Left atrial; PV = Pulmonary vein; PVI = Pulmonary vein isolation; PVs = Pulmonary veins; RF= Radiofrequency; SD = Standard deviation; WTI = Wall thickness index; WTI%= Wall thickness index percentage.

INTRODUCTION

Percutaneous pulmonary vein isolation (PVI) catheter ablation is a well-recognized treatment, with a class I indication, for symptomatic, drug-refractory atrial fibrillation (AF)^{1,2}. Unfortunately, despite more than 20 years of experience and significant technological developments, the efficacy of this procedure remains suboptimal^{3,4} and the associated risk of complications is still significant, albeit small^{5,6}.

One of the major limitations of the current technologies for percutaneous catheter ablation is the inability to provide real-time information on the LA wall thickness and on the acute tissue changes produced by energy delivery during ablation. Due to the unpredictable variability of the LA wall thickness in the areas targeted for ablation⁷⁻¹¹, choosing optimal ablation settings for achievement of transmural lesions is often challenging. Insufficient ablation will translate into non-transmural and non-durable lesions, while excessive ablation could lead to steam pops, cardiac perforation and damage to surrounding anatomical structures (e.g. the esophagus). Moreover, very little is known about acute tissue changes produced by catheter ablation and the role they might play in lesion failure. Acute development of tissue oedema has been reported when using radiofrequency (RF) energy for ablation¹²⁻¹⁴ and it has been advocated as a possible mechanism accounting for lesion failure^{15,16}. The presence and degree of acute tissue oedema when using cryoenergy or laser energy for ablation is not known.

Ultrasound imaging has previously been used in animal studies for assessment of atrial wall thickness and lesion formation during catheter ablation¹⁷⁻¹⁹. Preliminary data in human also suggest that ultrasound imaging modalities such as intracardiac echocardiography (ICE) and intravascular ultrasound (IVUS) can be used for LA wall thickness measurements and can detect acute changes produced by ablation^{20,21}.

This pilot study was conducted to compare ICE and IVUS for real-time LA wall imaging and assessment of acute tissue changes produced by different ablation modalities such as RF, cryoablation and laser.

METHODS

Study design

The INSIDE PVs study (INtra-procedural ultraSound Imaging for DEtermination of atrial wall thickness and acute tissue changes after isolation of the Pulmonary Veins with radiofrequency, cryoballoon or laser balloon energy) was a single-center prospective pilot study. The trial was approved by the Local Ethics Committee, complied with the Declaration of Helsinki and was registered on www.clinicaltrials.gov (Identifier NCT03372798).

Patients scheduled for RF, cryoballoon or laser balloon PVI catheter ablation for symptomatic, drug-refractory paroxysmal AF were eligible for the trial. As part of the trial, PV imaging was performed with ICE or IVUS before and after PVI. All AF ablations were performed in a standard fashion. Study design, ablation and imaging protocols and statistical analysis are detailed in the supplementary section.

Offline ICE/IVUS quantitative images analysis

Images were stored and analyzed offline by two independent operators, blinded to clinical and procedural data at the OxACCT CoreLab (Oxford Academic Cardiovascular CT CoreLab) using QIVUS software (Medis Medical, Leiden, The Netherlands). Image analysis was performed as previously outlined in the American College of Cardiology and European Society of Cardiology expert consensus document on the standards of IVUS imaging of vessels²² and specifically applied to the PVs¹¹.

Lumen and vessel diameters, areas and sphericity indices and wall thickness were measured at the level of the PV ostium as indicated in Figure 1.

Comparisons between corresponding PVs measurements obtained from ICE and IVUS frames and between pre- and post-ablation measurements were made. The impact of the different ablation technologies (RF, cryoballoon or laser balloon) on acute wall changes was also assessed. Post-ablation morphological changes of the PV wall such as dissection-like changes were recorded.

Assessment of performance of ICE and IVUS

The time required for imaging and any procedural complications associated with imaging were recorded as indicators of trackability of ICE and IVUS catheters.

The quality of imaging for each PV cross-section was defined as good, satisfactory, sub-optimal and poor, as indicated in the supplementary section.

The inter-observer agreement for quantitative data was also assessed for both ICE and IVUS by calculating intra-class correlation coefficient (ICC) values for different PV measurements.

Follow-up data

Although the study was not designed to assess and compare clinical outcomes, long-term data were obtained from standard clinical follow-up appointments. The need of redoing catheter ablation due to recurrence of atrial tachyarrhythmias and which PVs were found to be reconnected at the redo procedure were reported.

RESULTS

Study population

Twelve patients undergoing PVI catheter ablation for paroxysmal AF were enrolled in the study. The patients' baseline characteristics are presented in Table 1.

Pulmonary vein isolation was performed with RF in 5 patients (20 PVs), with cryoballoon in 4 patients (16 PVs) and with laser balloon in 3 patients (12 PVs). All 48 PVs were isolated. A

total of 28 PVs in 7 patients were imaged before and after PVI with ICE, while 20 veins in 5 patients were imaged with IVUS.

Performance of ICE/IVUS for PVs imaging

No significant differences in terms of trackability were observed between ICE and IVUS catheters (additional procedural time required for imaging: ICE = 24.8 ± 3.4 min, IVUS = 25 ± 3.5 min, $p = 0.95$; no procedural complications).

As showed in Table 2, ICE showed a higher imaging quality than IVUS ($\chi^2 = 35,415$; $p < 0.001$).

Compared to IVUS, ICE also performed better in terms of inter-observer reproducibility of PV measurements, as showed in Table A of the supplementary section. Although both techniques showed excellent ICC values for PV lumen measurements, IVUS showed only moderate ICC values for PV vessel and wall thickness measurements, as compared to good and excellent ICC values exhibited by ICE for corresponding measurements.

ICE/IVUS images analysis

Out of the 48 PV cross-sections, 3 were discarded because of poor quality and 45 (28 ICE and 17 IVUS frames) were considered adequate for quantitative analysis.

Compared to the IVUS cross-sections, the ICE ones showed larger lumen and vessel diameters and areas, larger wall thicknesses and significantly lower lumen and vessel sphericity indices, indicative of more oval/elliptical shape of both lumen and vessel contours (Table 3). Of note, median pre- and post-ablation wall thickness index percentage (WTI%) and muscular sleeve thicknesses did not differ between ICE and IVUS-imaged PVs.

As detailed in Table 4, statistically significant increases in mean wall thickness, wall thickness index (WTI) and WTI%, suggestive of acute wall thickening, were observed after ablation in both ICE and IVUS cross-sections. A significant reduction of the thickness of the muscular sleeve was also observed after ablation [ICE cross-sections: median (IQR) percentage reduction = 8.2% (0-45.9); IVUS cross-sections: median (IQR) percentage reduction = 31.68% (14.54-81.64)], with complete disappearance of the muscular sleeve after ablation in 6 PVs out of 45.

When grouping by ablation technology used for PVI (RF, cryo or laser), the increase in WTI% was observed only after RF treatment ($p = 0.003$) and laser treatment ($p = 0.003$), whilst no significant changes in wall thickness were observed after cryo ablation ($p = 0.69$) (Figure 2, Table 5).

A single case of vessel dissection was documented after ablation (right inferior pulmonary vein after cryoballoon ablation) (Figure 3).

Follow-up data

Patients were followed up for 26.5 ± 4.1 months. 6 patients (50%) required a redo procedure due to recurrence of atrial tachyarrhythmias 3 months or later after the AF ablation. Among them, 67% (4 patients) had reconnected PVs, for a total of 7 reconnected PVs out of the 24 checked during the redo procedures.

Reconnected and isolated PVs at the second ablation procedure had showed similar degrees of wall thickness increase [median (IQR) WTI% increase: reconnected PVs = 5.71% (0.31-12.04); isolated PVs = 4.51% (0.94-12.07); $p = 0.89$] and muscular sleeve thickness reduction after the first ablation procedure [median (IQR) percentage reduction: reconnected PVs = 8.72% (0.3-44.5); isolated PVs = 24.53% (0.5-41.18); $p = 0.58$].

DISCUSSION

Our pilot study was conducted to compare ICE and/or IVUS for real-time LA wall imaging and for detection of acute tissue changes produced by different ablation modalities. Although both ICE and IVUS probes image in the axial plan, providing cross-sectional images of the vessel (or chamber of interest) and surrounding tissues, their transducers use different ranges of ultrasound frequencies. The catheter designs are also different: the IVUS catheter has a smaller size (6F) and uses a mono-rail system, with the distal portion of the catheter advanced over a guidewire for better support and stability, while the ICE catheter has a bigger size (9F) and no central lumen. We chose to compare a 9MHz ICE catheter with a 20MHz IVUS probe to investigate which ultrasound frequency would give the best compromise between contrast resolution and image penetration for PVs imaging.

In our study, ICE performed better than IVUS with regards to quality of imaging provided and to inter-observer reproducibility of measurements obtained. These findings are likely due to the lower ultrasound frequency used by ICE, which was advantageous in terms of acoustic penetration without a significant loss in spatial resolution. When using ICE, the outer vessel circumference was well-defined in most or all image quadrants, as well as inner structures such as lumen circumference and wall.

We observed no significant differences between the two technologies in terms of trackability: similar additional procedural times were needed for ICE and for IVUS imaging and no procedural complications occurred as result of imaging.

Both lumen and vessel diameters and areas were consistently larger in the ICE-imaged PVs compared to the IVUS-imaged PVs. Moreover, although both imaging techniques showed an elliptical shape of the PV cross-sections, in keeping with previous CT and MRI studies^{23,24}, lumen and vessel sphericity indices were lower in the ICE-imaged PVs, which is indicative of a more elliptical shape of the PV cross-sections. Our PVs measurements determined by IVUS are in line with previously reported PV measurements, obtained from both IVUS images and histological sections¹¹. Putting together, these data might suggest that ICE overestimated the PVs sizes due to non-coaxial cross-sectioning, as indicated by the lower sphericity index when compared to the IVUS images. ICE catheters are not advanced or pulled back over a wire and this different design might have reduced the chance of a coaxial position of the probe within the PV lumen. Despite different lumen and vessel diameters and absolute areas, pre- and post-ablation WTI% were comparable between PV cross-sections imaged

either ICE or IVUS, thus suggesting that both imaging modalities can provide similar accuracy in depicting acute changes in tissue thickness after ablation.

In our study, the LA wall thickness was found to increase at the level the PV ostia following ablation when using RF or laser balloon energy, while no increase in wall thickness was observed when using the cryoballoon. While acute development of tissue oedema is well known after RF^{18,25,26}, very limited data are available regarding acute tissue changes after laser energy delivery^{27,28}. Apart from the lack of direct contact of the energy source with the tissue (the optical fiber delivering arc of laser energy is in a balloon), laser energy as RF produces tissue damage through heating and it is delivered in a point-by-point fashion. Thus, it is not surprising that the two energy modalities might share similar mechanisms of tissue injury, including acute wall thickness increase from oedema as shown by our study.

The acute tissue changes produced by cryoablation were previously investigated with IVUS in another study²⁰. The same type of cryoballoon catheter was used for ablation and a similar number of freezes was delivered in each vein. In contrast with our findings, PVs imaging after cryoablation showed tissue oedema in 90% of the PVs, extending from the ostium up to 3 cm distally. Of note, in the same study, dissection-like changes were observed, together with oedema, in most of the PVs; while in our study, dissection-like changes were observed only in one vein after cryoballoon ablation and, interestingly, this occurred in the context of acute wall tissue thickening. It could be hypothesized that in these veins the oedema was related to a reaction of the vessel wall following the mechanical injury associated with dissection, rather than being a direct consequence of cryoenergy delivery. In the sequential process of tissue injury produced by cryoenergy^{29,30}, tissue oedema is supposed to occur only at a late stage, once the tissue has thawed, following freezing, and has become hyperaemic, and to gradually progress over the next hours³¹. Concordantly, early PV imaging in our study showed no acute wall thickening suggestive of development of oedema.

The different morphological changes produced by the different ablation energies could suggest different mechanisms of lesion failure. Recent data suggest that the adjustment of the ablation settings based on baseline LA wall thickness can improve the procedure outcome and reduce the risk of collateral injury²¹. A further adjustment based on the acute wall thickening produced by energy delivery for ablation could also be beneficial when using RF or laser energy.

Apart from acute wall thickening, we observed a reduction of the thickness of the PV muscular sleeve after PVI catheter ablation. Myocardial sleeves are known to extend from the left atrium into the PVs walls and to be source of focal activity triggering AF³². The thickness reduction after ablation could indicate damage, translating to elimination of the PVs potentials and acute electrical isolation of the vein and may also explain why it is often impossible to get local capture during pacing to demonstrate exit-block. Whether a durable PV isolation correlates with a certain degree of wall thickness reduction or complete disappearance of the muscular sleeve after catheter ablation is unclear. We did not observe a correlation between degree of wall thickness increase or muscular sleeve thickness reduction after the first catheter ablation procedure and evidence of PV reconnection at the second catheter ablation procedure; however, only a small number of PVs was checked with a second ablation procedure in our study.

Limitations

There are some limitations in our work that must be acknowledged. First, results need to be interpreted as hypothesis-generating and in light of the small and heterogeneous sample size, due to the use of different imaging modalities and different ablation modalities.

No direct comparisons between ICE and IVUS were made by imaging the same PVs with both modalities. No other imaging modality or histopathology was available as reference for the PVs measurements obtained with ICE and IVUS to ascertain which of the two imaging modalities gave more accurate measurements. However, this did not preclude confirming the feasibility of both ICE and IVUS for LA wall imaging, since comparable wall thickness measurements were obtained and similar acute changes in wall thickness were detected with both imaging modalities.

Pullback was manual rather than automatic. This precluded the precise comparison of distal cross-sections before and after ablation.

Imaging during energy delivery was not attempted, as the same trans-septal access was used for either ablation catheter or imaging catheter. However, it might be that simultaneous imaging would have not been possible due to spatial interference, especially when using cryo or laser balloon catheters, and/or due to artifacts created by irrigation of the RF catheter.

CONCLUSIONS

In our pilot study, ICE performed better than IVUS with regards to imaging quality and inter-observer reproducibility of measurements obtained. Acute wall thickening was observed at the PV ostia after RF and laser energy delivery and not after cryoenergy delivery. Larger studies are needed to confirm these preliminary findings and their potential clinical implications.

ACKNOWLEDGEMENTS

We thank the John Radcliffe Hospital Cardiac Angiography Suite Team and the Oxford Cardiac Research Team for their invaluable help and support for the conduction of the study.

FUNDING

Prof. Betts is supported by the Oxford NIHR Biomedical Research Centre. Dr Leo's salary was supported by an unrestricted research grant from Abbott Medical.

REFERENCES

1. Calkins H. 2017 HRS/EHRA/ECAS/APHRS/SOLAECE expert consensus statement on catheter and surgical ablation of atrial fibrillation. *Heart rhythm* 2017;14:170.
2. Hindricks G Fau - Potpara T, Potpara T Fau - Dagres N, Dagres N Fau - Arbelo E, et al. 2020 ESC Guidelines for the diagnosis and management of atrial fibrillation developed in collaboration with the European Association for Cardio-Thoracic Surgery (EACTS).
3. Cheema A, Dong J, Dalal D, et al. Incidence and time course of early recovery of pulmonary vein conduction after catheter ablation of atrial fibrillation. *Journal of cardiovascular electrophysiology* 2007;18:387-91.
4. Cappato R, Negroni S, Pecora D, et al. Prospective assessment of late conduction recurrence across radiofrequency lesions producing electrical disconnection at the pulmonary vein ostium in patients with atrial fibrillation. *Circulation* 2003;108:1599-604.
5. Gupta A, Perera T, Ganesan A, et al. Complications of catheter ablation of atrial fibrillation: a systematic review. *Circulation Arrhythmia and electrophysiology* 2013;6:1082-8.
6. Cappato R, Calkins H, Chen S-A, et al. Updated Worldwide Survey on the Methods, Efficacy, and Safety of Catheter Ablation for Human Atrial Fibrillation. *Circulation: Arrhythmia and Electrophysiology* 2010;3:32-8.
7. Hall B, Jeevanantham V, Simon R, Filippone J, Vorobiof G, Daubert J. Variation in left atrial transmural wall thickness at sites commonly targeted for ablation of atrial fibrillation. *J Interv Card Electrophysiol* 2006;17:127-32.
8. Whitaker J, Rajani R, Chubb H, et al. The role of myocardial wall thickness in atrial arrhythmogenesis. *Europace : European pacing, arrhythmias, and cardiac electrophysiology : journal of the working groups on cardiac pacing, arrhythmias, and cardiac cellular electrophysiology of the European Society of Cardiology* 2016;18:1758-72.
9. Ho SY, Sanchez-Quintana D, Cabrera JA, Anderson RH. Anatomy of the left atrium: implications for radiofrequency ablation of atrial fibrillation. *Journal of cardiovascular electrophysiology* 1999;10:1525-33.
10. Ho SY, Cabrera JA, Sanchez-Quintana D. Left atrial anatomy revisited. *Circulation Arrhythmia and electrophysiology* 2012;5:220-8.
11. Cabrera JA, Sánchez-Quintana D, Farré J, et al. Ultrasonic characterization of the pulmonary venous wall: echographic and histological correlation. *Circulation* 2002;106:968-73.
12. Schwartzman D, Ren JF, Devine WA, Callans DJ. Cardiac swelling associated with linear radiofrequency ablation in the atrium. *J Interv Card Electrophysiol* 2001;5:159-66.
13. Weerasooriya R, Jaïs P, Sanders P, et al. Images in cardiovascular medicine. Early appearance of an edematous tissue reaction during left atrial linear ablation using intracardiac echo imaging. *Circulation* 2003;108:e80.
14. Okada T, Yamada T, Murakami Y, et al. Prevalence and Severity of Left Atrial Edema Detected by Electron Beam Tomography Early After Pulmonary Vein Ablation. *J Am Coll Cardiol* 2007;49:1436-42.
15. Yamada T, Murakami Y, Okada T, et al. Incidence, location, and cause of recovery of electrical connections between the pulmonary veins and the left atrium after pulmonary vein isolation. *Europace : European pacing, arrhythmias, and cardiac electrophysiology : journal of the working groups on cardiac pacing, arrhythmias, and cardiac cellular electrophysiology of the European Society of Cardiology* 2006;8:182-8.
16. Arujuna A, Karim R, Caulfield D, et al. Acute pulmonary vein isolation is achieved by a combination of reversible and irreversible atrial injury after catheter ablation: evidence from magnetic resonance imaging. *Circulation Arrhythmia and electrophysiology* 2012;5:691-700.
17. Ren JF, Callans DJ, Schwartzman D, Michele JJ, Marchlinski FE. Changes in local wall thickness correlate with pathologic lesion size following radiofrequency catheter ablation: an intracardiac echocardiographic imaging study. *Echocardiography* 2001;18:503-7.

18. Granier M, Winum PF, Granier M, et al. Real-time atrial wall imaging during radiofrequency ablation in a porcine model. *Heart rhythm* 2015;12:1827-35.
19. Ren JF, Callans DJ, Schwartzman D, Michele JJ, Marchlinski FE. Changes in local wall thickness correlate with pathologic lesion size following radiofrequency catheter ablation: an intracardiac echocardiographic imaging study. *Echocardiography* 2001;18:503-7.
20. Baran J, Lewandowski P, Smarż K, Sikorska A, Zaborska B, Kułakowski P. Acute Hemodynamic and Tissue Effects of Cryoballoon Ablation on Pulmonary Vessels: The IVUS-Cryo Study. *J Am Heart Assoc* 2017;6.
21. Motoike Y, Harada M, Ito T, et al. Wall Thickness-Based Adjustment of Ablation Index Improves Efficacy of Pulmonary Vein Isolation in Atrial Fibrillation: Real-Time Assessment by Intracardiac Echocardiography. *Journal of cardiovascular electrophysiology* 2021.
22. Mintz GS, Nissen SE, Anderson WD, et al. American College of Cardiology Clinical Expert Consensus Document on Standards for Acquisition, Measurement and Reporting of Intravascular Ultrasound Studies (IVUS). A report of the American College of Cardiology Task Force on Clinical Expert Consensus Documents. *J Am Coll Cardiol* 2001;37:1478-92.
23. Jongbloed MR, Bax JJ, Lamb HJ, et al. Multislice computed tomography versus intracardiac echocardiography to evaluate the pulmonary veins before radiofrequency catheter ablation of atrial fibrillation: a head-to-head comparison. *J Am Coll Cardiol* 2005;45:343-50.
24. Wittkamp FH, Vonken EJ, Derksen R, et al. Pulmonary vein ostium geometry: analysis by magnetic resonance angiography. *Circulation* 2003;107:21-3.
25. Haines DE, Wright M, Harks E, et al. Near-Field Ultrasound Imaging During Radiofrequency Catheter Ablation: Tissue Thickness and Epicardial Wall Visualization and Assessment of Radiofrequency Ablation Lesion Formation and Depth. *Circulation Arrhythmia and electrophysiology* 2017;10.
26. Wright M, Harks E, Deladi S, et al. Characteristics of Radiofrequency Catheter Ablation Lesion Formation in Real Time In Vivo Using Near Field Ultrasound Imaging. *JACC Clinical electrophysiology* 2018;4:1062-72.
27. Reddy VY, Neuzil P, Themistoclakis S, et al. Visually-guided balloon catheter ablation of atrial fibrillation: experimental feasibility and first-in-human multicenter clinical outcome. *Circulation* 2009;120:12-20.
28. Gerstenfeld EP, Michele J. Pulmonary vein isolation using a compliant endoscopic laser balloon ablation system in a swine model. *J Interv Card Electrophysiol* 2010;29:1-9.
29. Khairy P, Dubuc M. Transcatheter cryoablation part I: preclinical experience. *Pacing and clinical electrophysiology : PACE* 2008;31:112-20.
30. Lustgarten DL, Keane D, Ruskin J. Cryothermal ablation: mechanism of tissue injury and current experience in the treatment of tachyarrhythmias. *Progress in cardiovascular diseases* 1999;41:481-98.
31. Gage AA, Baust J. Mechanisms of tissue injury in cryosurgery. *Cryobiology* 1998;37:171-86.
32. de Bakker JM, Ho Sy Fau - Hocini M, Hocini M. Basic and clinical electrophysiology of pulmonary vein ectopy.

TABLES

Table 1. Patients' baseline characteristics

| | |
|---|-----------------|
| Total number of patients | 12 |
| Age (years), mean \pm SD | 64.8 \pm 11.8 |
| Sex (males), number of patients (%) | 4 (33%) |
| LA volume index (ml/m²), mean \pm SD | 28.6 \pm 4.6 |
| LV systolic function (%), mean \pm SD | 57.1 \pm 6.6 |

Legend: LA= left atrial; LV= left ventricular; SD= standard deviation.

Table 2. Imaging quality: comparison between ICE and IVUS.

| | ICE | IVUS |
|--|----------|----------|
| Image Quality , number of PV runs (%) | | |
| Good | 24 (86%) | 0 (0%) |
| Satisfactory | 4 (14%) | 13 (65%) |
| Sub-optimal | 0 (0%) | 4 (20%) |
| Poor | 0 (0%) | 3 (15%) |
| Total | 28 | 20 |

Table 3. PVs measurements obtained with ICE/IVUS before and after PVI catheter ablation: comparison between ICE- and IVUS-imaged PVs.

| | ICE imaging | IVUS imaging | p |
|---|---------------------|--------------------|--------------------|
| PRE-ABLATION | | | |
| Mean lumen diameter (mm), mean \pm SD | 18.57 \pm 3.77 | 10.96 \pm 2.24 | < 0.0001 |
| Maximum lumen diameter (mm), mean \pm SD | 22.23 \pm 4.85 | 12.2 \pm 2.76 | < 0.0001 |
| Minimum lumen diameter (mm), mean \pm SD | 15.69 \pm 3.58 | 9.89 \pm 2.09 | < 0.0001 |
| Lumen sphericity index, mean \pm SD | 0.72 \pm 0.14 | 0.82 \pm 0.11 | 0.012 |
| Lumen area (mm ²), mean \pm SD | 281.46 \pm 115.06 | 98.05 \pm 36.74 | < 0.0001 |
| Mean vessel diameter (mm), mean \pm SD | 21.21 \pm 3.72 | 12.58 \pm 2.5 | < 0.0001 |
| Maximum vessel diameter (mm), mean \pm SD | 24.57 \pm 4.78 | 13.61 \pm 2.90 | < 0.0001 |
| Minimum vessel diameter (mm), mean \pm SD | 18.36 \pm 3.50 | 11.69 \pm 2.42 | < 0.0001 |
| Vessel sphericity index, mean \pm SD | 0.76 \pm 0.13 | 0.87 \pm 0.09 | 0.005 |
| Vessel area (mm ²), mean \pm SD | 363.84 \pm 130.33 | 129.02 \pm 47.34 | < 0.0001 |
| Muscular sleeve thickness (mm), median (IQR) | 0.55 (0.34- 0.70) | 0.35 (0.11-0.60) | 0.12 |
| Mean wall thickness (mm), median (IQR) | 1.18 (0.95-1.52) | 0.78 (0.67-0.84) | < 0.0001 |
| Maximum wall thickness (mm), median (IQR) | 2.02 (1.62-3.03) | 1.36 (1.09-1.52) | < 0.0001 |
| Minimum wall thickness (mm), median (IQR) | 0.41 (0.25-0.63) | 0.26 (0.22-0.32) | 0.04 |
| WTI (mm ²), median (IQR) | 73.39 (55.79-109.5) | 29.67 (24.4-33.9) | < 0.0001 |
| WTI% (%), median (IQR) | 22.18 (16.4-29.1) | 23.15 (20.8-27.8) | 0.51 |
| POST-ABLATION | | | |
| Mean lumen diameter (mm), mean \pm SD | 18.3 \pm 3.97 | 10.93 \pm 2.16 | < 0.0001 |
| Maximum lumen diameter (mm), mean \pm SD | 22.45 \pm 4.82 | 12.29 \pm 2.41 | < 0.0001 |
| Minimum lumen diameter (mm), mean \pm SD | 14.75 \pm 4.27 | 9.85 \pm 2.21 | < 0.0001 |
| Lumen sphericity index, mean \pm SD | 0.66 \pm 0.13 | 0.81 \pm 0.12 | 0.004 |
| Lumen area (mm ²), mean \pm SD | 275.48 \pm 118.24 | 97.36 \pm 34.64 | < 0.0001 |
| Mean vessel diameter (mm), mean \pm SD | 21.54 \pm 3.94 | 12.95 \pm 2.39 | < 0.0001 |

| | | | |
|---|--------------------|-------------------|--------------------|
| Maximum vessel diameter (mm), mean ± SD | 25.18 ± 5.1 | 14.06 ± 2.72 | < 0.0001 |
| Minimum vessel diameter (mm), mean ± SD | 18.36 ± 3.53 | 11.99 ± 2.37 | < 0.0001 |
| Vessel sphericity index, mean ± SD | 0.74 ± 0.13 | 0.86 ± 0.1 | 0.003 |
| Vessel area (mm²), mean ± SD | 374.56 ± 139.38 | 136.00 ± 46.33 | < 0.0001 |
| Muscular sleeve thickness (mm), median (IQR) | 0.37 (0.33-0.51) | 0.22 (0.01-0.46) | 0.39 |
| Mean wall thickness (mm), median (IQR) | 1.52 (1.20-1.90) | 0.93 (0.76-1.11) | < 0.0001 |
| Maximum wall thickness (mm), median (IQR) | 2.52 (1.99-3.64) | 1.58 (1.23-2.0) | < 0.0001 |
| Minimum wall thickness (mm), median (IQR) | 0.51 (0.29-0.80) | 0.40 (0.28-0.56) | 0.276 |
| WTI (mm²), median (IQR) | 94.38 (71.0-132.6) | 39.12 (25.9-44.8) | < 0.0001 |
| WTI% (%), median (IQR) | 27.01 (20.6-34.4) | 27.09 (22.8-32.3) | 0.85 |

Legend: IQR= interquartile range; SD= standard deviation; WTI= wall thickness index; WTI%= wall thickness index %.

Table 4. Comparison between pre and post ablation PV measurements in the ICE- and in the IVUS-imaged veins.

| | ICE imaged PVs | | | IVUS imaged PVs | | |
|--|--------------------------|-------------------------|--------------|------------------------|------------------------|---------------|
| | Pre-ablation | Post-ablation | p | Pre-ablation | Post-ablation | p |
| Mean lumen diameter (mm), mean \pm SD | 18.57 \pm 3.77 | 18.3 \pm 3.97 | 0.557 | 10.96 \pm 2.24 | 10.93 \pm 2.16 | 0.893 |
| Lumen area (mm²), mean \pm SD | 281.46 \pm 115.06 | 275.48 \pm 118.24 | 0.673 | 98.05 \pm 36.74 | 97.36 \pm 34.64 | 0.834 |
| Mean vessel diameter (mm), mean \pm SD | 21.21 \pm 3.72 | 21.54 \pm 3.94 | 0.461 | 12.58 \pm 2.5 | 12.95 \pm 2.39 | 0.106 |
| Vessel area (mm²), mean \pm SD | 363.84 \pm 130.33 | 374.56 \pm 139.38 | 0.523 | 129.02 \pm 47.34 | 136.00 \pm 46.33 | 0.126 |
| Muscular sleeve thickness (mm), median (IQR) | 0.55 (0.34- 0.70) | 0.37 (0.33-0.51) | 0.001 | 0.35 (0.11-0.60) | 0.22 (0.01-0.46) | 0.034 |
| Mean wall thickness (mm), median (IQR) | 1.19 (0.95-1.52) | 1.52 (1.21-1.9) | 0.008 | 0.78 (0.67-0.84) | 0.93 (0.76-1.11) | 0.016 |
| WTI (mm²), median (IQR) | 73.39 (55.79 - 109.5) | 94.38 (71.0 - 132.6) | 0.006 | 29.67 (24.4 – 33.9) | 39.12 (25.9 – 44.8) | 0.006 |
| WTI% (%), median (IQR) | 22.18 (16.4 - 29.1) | 27.01 (20.6 – 34.4) | 0.012 | 23.15 (20.8 - 27.8) | 27.09 (22.8 – 32.3) | 0.0025 |

Legend: IQR= interquartile range; SD= standard deviation; WTI= wall thickness index; WTI%= wall thickness index %.

Table 5. Acute changes produced by catheter ablation: comparison among different PVI ablation technologies.

| | RF (18 PVs) | Cryo (15 PVs) | Laser (12 PVs) |
|---|--------------------------|---------------------------------------|--------------------------|
| Mean application time per vein | 13.1 ± 2.1 min | 1.9 ± 0.6 freezes (360 ± 95.5 sec) | 19.5 ± 1.5 min |
| WTI% (%), median (IQR) | | | |
| Pre-ablation | 21.21 (15.48 - 23.68) | 25.06 (22.30 - 31.57) | 25.30 (19.62- 29.93) |
| Post-ablation | 25.83 (19.71- 31.39) | 24.33 (20.45 – 32.02) | 31.97 (26.92 – 36.98) |
| p | 0.003 | 0.69 | 0.003 |
| Muscular sleeve thickness (mm), median (IQR) | | | |
| Pre-ablation | 0.36 (0.20-0.64) | 0.35 (0.01-0.56) | 0.65 (0.45-1.32) |
| Post-ablation | 0.24 (0.02-0.44) | 0.25 (0.0-0.52) | 0.39 (0.0-0.55) |
| p | 0.037 | 0.005 | 0.008 |

Legend: IQR= interquartile range; RF= radiofrequency energy; WTI% = Wall Thickness Index %.

FIGURES LEGEND

Figure 1. Analyses conducted on PV os frames: wall structures identified and measurements calculated (*in italic*).

Figure 2. Wall thickness index % (WTI%) before and after ablation: comparison among different ablation technologies for Pulmonary Vein Isolation (PVI).

Figure 3. ICE image of os of same right inferior pulmonary vein, before (left panel) and after cryoablation (right panel). The white arrow indicates acute tissue thickening suggestive of oedema, while the white asterisks indicate a dissection flap.

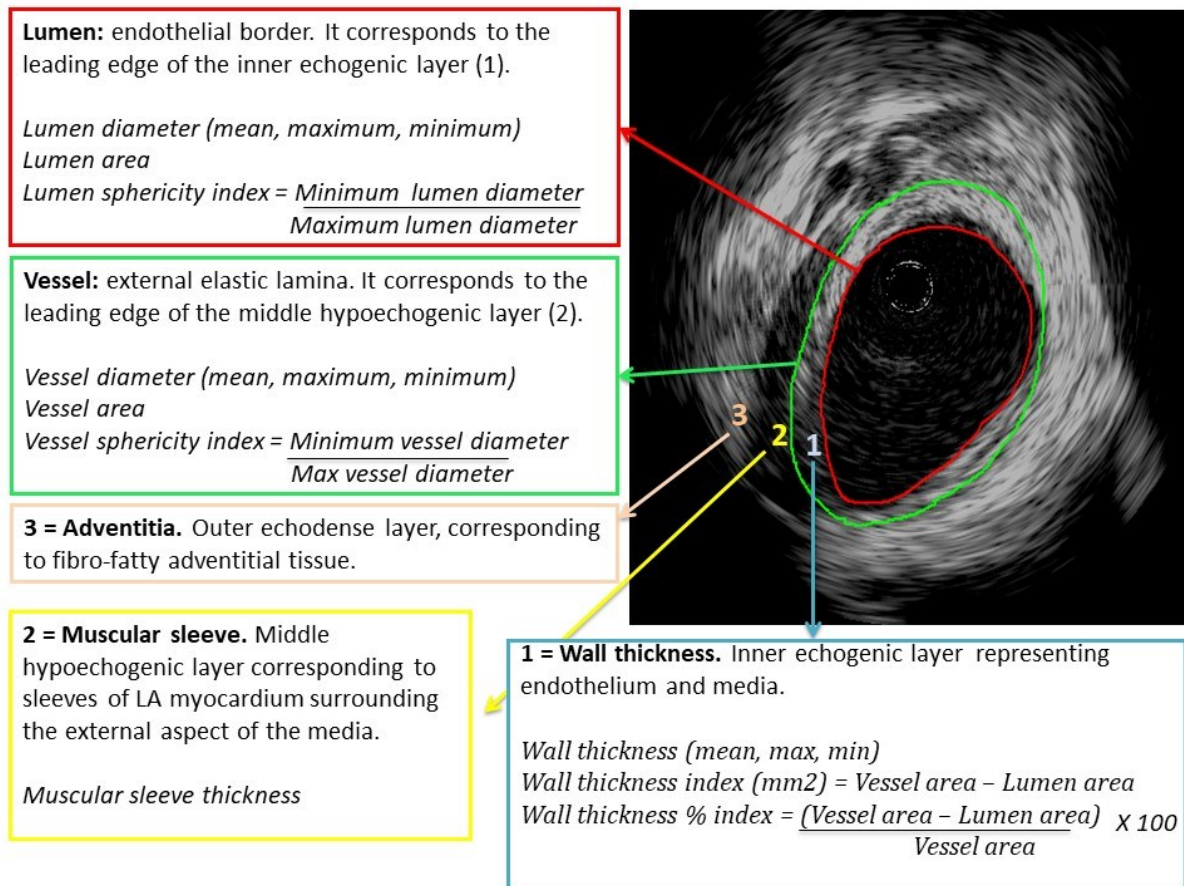


Figure 1. Analyses conducted on PV os frames: wall structures identified and measurements calculated (in italic).

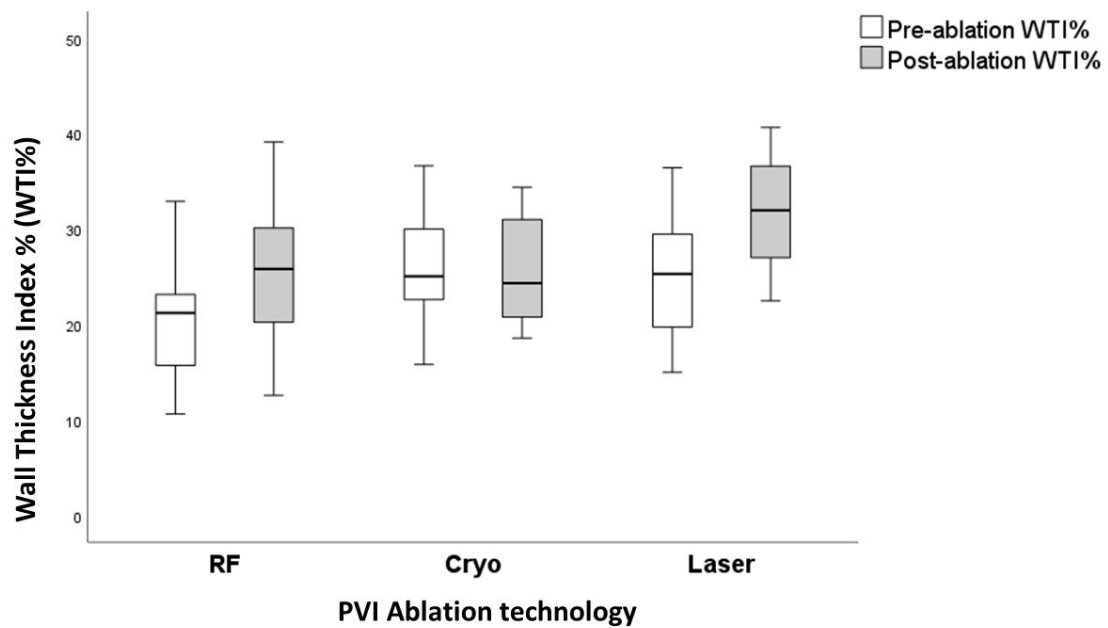


Figure 2. Wall thickness index % (WTI%) before and after ablation: comparison among different ablation technologies for Pulmonary Vein Isolation (PVI).

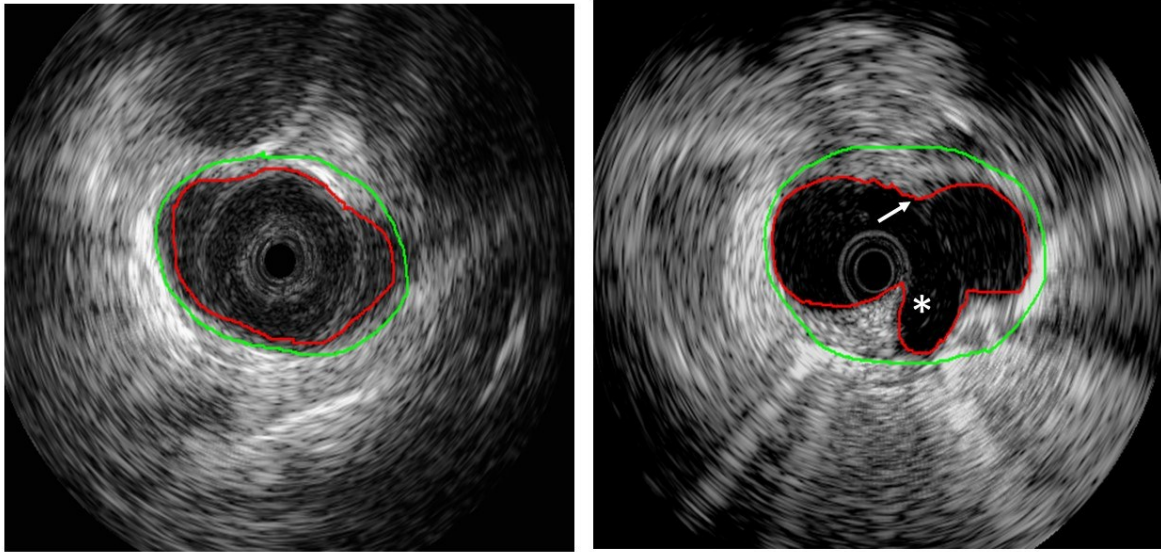


Figure 3. ICE image of os of same right inferior pulmonary vein, before (left panel) and after cryoablation (right panel). The white arrow indicates acute tissue thickening suggestive of oedema, while the white asterisk indicates a dissection flap.

SUPPLEMENTARY SECTION

METHODS

Study design

In addition to procedural LA and PVs imaging with ICE or IVUS, the study design also included pre-procedural and early post-procedural (within 24 hour from the ablation procedure) imaging with cardiac Computed Tomography (CT). The aim was to use the cardiac CT as gold standard for measurement of PV ostial diameters and LA wall thickness at the PVs junctions, both at baseline and shortly after ablation, and compare the CT measurements with the corresponding ICE and IVUS measurements to assess their accuracy. Unfortunately, the CT images were inadvertently deleted by a third party before any analysis was performed; hence the CT data are not reported as not available.

Atrial fibrillation ablation protocols

All AF ablations were performed in a standard fashion on uninterrupted therapeutic anticoagulation. After general anaesthesia and oro-tracheal intubation, transoesophageal echocardiography was performed to rule out the presence of thrombus. After femoral venous access, LA access was obtained through one or two atrial trans-septal punctures performed under fluoroscopic and trans-oesophageal guidance. Heparin was administered to achieve and maintain Activated Clotting Time (ACT) values of 300-400 seconds throughout the procedure. Radiofrequency (RF) energy, cryoballoon or laser balloon were used for PVI as per operator preference.

When using RF energy, a 3D electroanatomic mapping system was used (EnSite Velocity, Abbott Medical, St Paul, MN, USA or CARTO mapping system, Biosense Webster, Inc, CA) to construct the LA and PVs geometry with a circular mapping catheter (Optima, Abbott Medical, St Paul, MN, USA or Lasso, Biosense Webster, Inc, CA, respectively). An irrigated-tip contact force sensing ablation catheter (Tacticath Quartz, Abbott Medical, St Paul, MN, USA or Thermocool SmartTouch, Biosense Webster, Inc, CA) was used for ablation through a deflectable sheath (Agilis, Abbott Medical, St Paul, MN, USA). Wide area antral PVI was performed in all patients using point-by-point ablation, with delivery of contiguous lesions on a predetermined encirclement. A 40W power was used for ablation, aiming at a minimum contact force of 10 gr and targeting Lesion Size Index (LSI) values of 5/Ablation Index (AI) values of 400 posteriorly and LSI values of 6/AI values of 550 anteriorly. The left and right veins were treated as pairs, with additional ablation performed at the carina between upper and lower veins if circumferential encirclement failed to isolate both veins. Pulmonary Vein Isolation was confirmed by disappearance of PV potentials or evidence of dissociated PV potentials and PV entrance and exit block with pacing.

When using cryoenergy, LA and PV angiography were performed to delineate anatomy. A FlexCath (Medtronic, Minneapolis, MN, USA) was advanced to the LA and used to deliver a

28 mm Arctic Front Advance cryoablation balloon (Medtronic, Minneapolis, MN, USA). The balloon was inflated at the ostium of each PV. After retrograde PV angiography, to demonstrate PV occlusion, one or more 4-minute freezes were performed in each PV until PVI was achieved. Pulmonary Vein Isolation was confirmed by disappearance of PV potentials or evidence of dissociated PV potentials and PV entrance and exit block with pacing, by using an Achieve guidewire (Medtronic, Minneapolis, MN, USA).

When using laser energy, a laser balloon system (HeartLight, CardioFocus) was delivered to the LA through a 12-F deflectable sheath and inflated at the ostium of each PV. Ablation lesions were delivered in a circumferential, contiguous, and overlapping manner around the PV using 5–12 W power whilst simultaneously undertaking oesophageal temperature monitoring. Pulmonary Vein isolation was confirmed by disappearance of PV potentials or evidence of dissociated PV potentials and PV entrance and exit block with pacing, by using an Achieve guidewire (Medtronic, Minneapolis, MN, USA).

Protocol for ICE/IVUS imaging of the PVs

Ultrasound imaging of the PVs-LA junctions was performed with either ICE or IVUS.

For ICE imaging, a 9F catheter with a 9 MHz rotational transducer providing a maximal radial depth of 50 mm (Ultra ICE, Boston Scientific) was used. For IVUS imaging, a 20 MHz digital probe with maximum ultrasonic detection depth of 24 mm (Visions PV .018, Volcano, San Diego, CA) was chosen and used mounted on a guidewire (0.014-in percutaneous transluminal coronary angioplasty guidewire) as per manufacture instructions.

In each patient one imaging modality between ICE and IVUS was selected, and choice left to operator's discretion and/or preference. All PVs were imaged per protocol. The ultrasound-imaging probe was introduced into the LA via the trans-septal access and advanced under fluoroscopic guidance distally into each PV with the aid of a long steerable sheath. Images were recorded during slow manual pull-back of the probe from each vein into the LA body. Each PV was imaged twice, before and after ablation. Consistent anatomical landmarks, such as the first bifurcation and the ridge between the left atrial appendage and the left PVs, were used as reference points to identify the ostium of each PV. The time required for imaging in each patient was recorded.

Assessment of quality of ICE/IVUS imaging

The imaging quality of each ICE/IVUS cross section was assessed and graded as good, satisfactory, sub-optimal or poor: good quality if the vessel contour was visible in all 4 quadrants; satisfactory quality if the vessel contour was visible in 3 quadrants; sub-optimal quality if the vessel contour was visible in 2 non-consecutive quadrants; poor quality if not possible to define the vessel contour as visible only in one quadrant or in two consecutive quadrants (Figure A). Cross-sections with image quality rated as "poor" were discarded and not considered for quantitative analyses.

Statistical analysis

Categorical variables were expressed as absolute number and percentage (%). Continuous variables were expressed as mean and (\pm) standard deviation (SD) or as median accompanied by interquartile range (IQR), as appropriate after checking for normality using the Shapiro-Wilk's test. Categorical variables were compared with the use of the Pearson's Chi-square test or Fisher's exact test, as appropriate. Continuous variables were compared with the use of one-way ANOVA test or Kruskal-Wallis test, as appropriate according to data distribution.

A two-sided P value of less than 0.05 was considered to indicate statistical significance. Data were analysed with the use of SPSS software version 27 (IBM Statistics, Chicago, Illinois).

RESULTS

Performance of ICE/IVUS for PV imaging: inter-observer reproducibility of measurements

Compared to IVUS, ICE performed better in terms of inter-observer reproducibility, as showed in Table A.

Table A. Intraclass Correlation (ICC) values of ICE and IVUS measurements.

| | ICE | IVUS |
|------------------------------------|-----------------------------|-----------------------------|
| Maximum lumen diameter | 0.98 (95% CI: 0.97–0.99) | 0.95 (95% CI: 0.90-0.98) |
| Minimum lumen diameter | 0.96 (95% CI: 0.91–0.98) | 0.94 (95% CI: 0.92-0.96) |
| Lumen area | 0.98 (95% CI: 0.97–0.99) | 0.95 (95% CI: 0.91-0.97) |
| Maximum vessel diameter | 0.93 (95% CI: 0.88-0.95) | 0.72 (95% CI: 0.60-0.93) |
| Minimum vessel diameter | 0.91 (95% CI: 0.87-0.93) | 0.73 (95% CI: 0.70-0.88) |
| Vessel area | 0.92 (95% CI: 0.89-0.95) | 0.71 (95% CI: 0.61-0.90) |
| Maximum wall thickness (mm) | 0.88 (95% CI: 0.83–0.88) | 0.70 (95% CI: 0.63-0.89) |
| Minimum wall thickness (mm) | 0.89 (95% CI: 0.81–0.89) | 0.69 (95% CI: 0.64-0.91) |

FIGURE LEGEND

Figure A. Grading of ICE/IVUS imaging quality, based on sharpness of the vessel contour in the 4 image quadrants. From left to right: examples of good quality, satisfactory quality and sub-optimal quality PV runs.

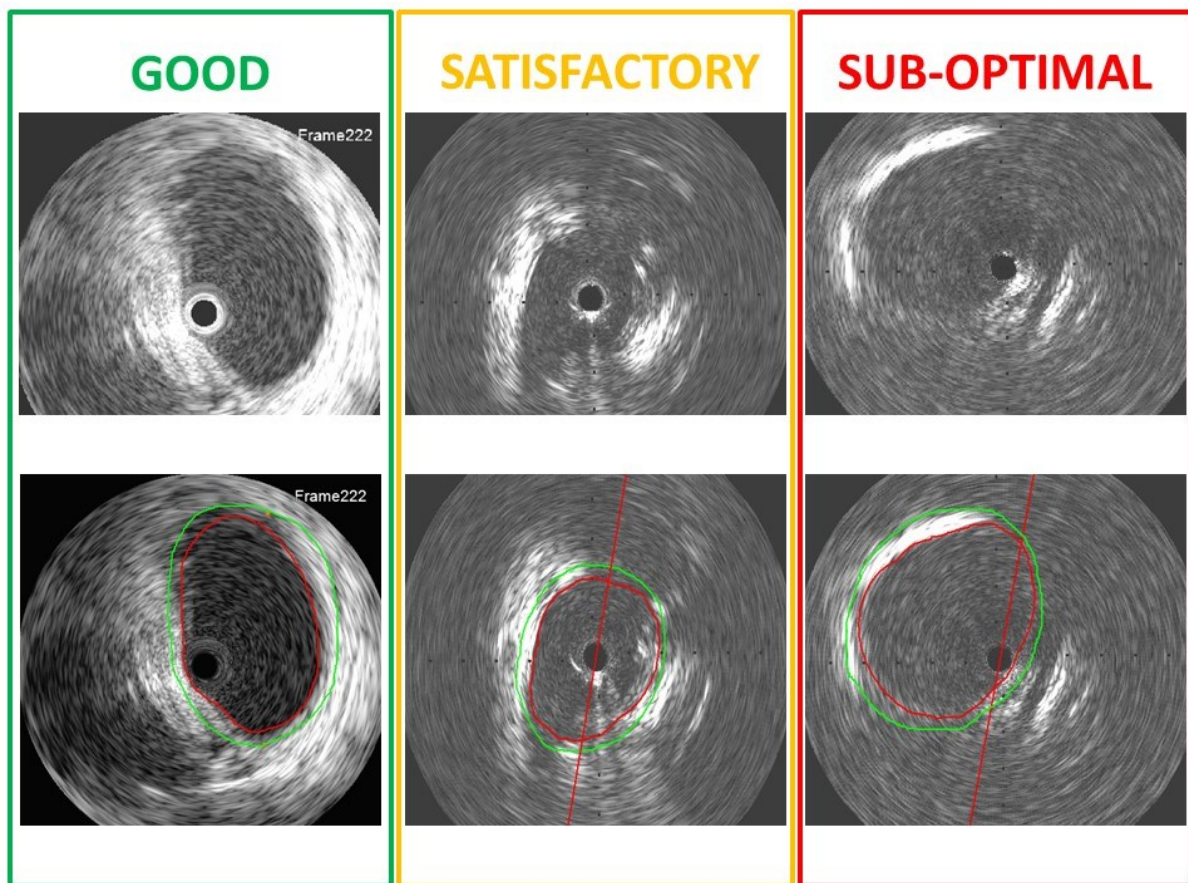


Figure A. Grading of ICE/IVUS imaging quality, based on sharpness of the vessel contour in the 4 image quadrants. From left to right: examples of good quality, satisfactory quality and sub-optimal quality PV cross-sections.